BIOCHEMISTRY
including biophysical chemistry & molecular biology

Article

pubs.acs.org/biochemistry

# Role of Glutamate 64 in the Activation of the Prodrug 5-Fluorocytosine by Yeast Cytosine Deaminase

Jifeng Wang,[†,§] Stepan Sklenak,[‡] Aizhuo Liu,[†] Krzysztof Felczak,[†,∥] Yan Wu,[†] Yue Li,[†] and Honggao Yan*[,†]

[†]Department of Biochemistry and Molecular Biology, Michigan State University, East Lansing, Michigan 48824, United States

[‡]J. Heyrovsky Institute of Physical Chemistry, Academy of Sciences of the Czech Republic, Dolejškova 3, 182 23 Prague, Czech Republic

Supporting Information

**ABSTRACT:** Yeast cytosine deaminase (yCD) catalyzes the hydrolytic deamination of cytosine to uracil as well as the deamination of the prodrug 5-fluorocytosine (5FC) to the anticancer drug 5-fluorouracil. In this study, the role of Glu64 in the activation of the prodrug 5FC was investigated by site-directed mutagenesis, biochemical, nuclear magnetic resonance (NMR), and computational studies. Steady-state kinetics studies showed that the mutation of Glu64 causes a dramatic decrease in $k_{cat}$ and a dramatic increase in $K_m$, indicating Glu64 is important for both binding and catalysis in the activation of 5FC. $^{19}$F NMR experiments showed that binding of the inhibitor 5-fluoro-1*H*-pyrimidin-2-one (5FPy) to the wild-type yCD causes an upfield shift, indicating that the bound inhibitor is in the hydrated form, mimicking the transition state or the tetrahedral intermediate in the activation of 5FC. However, binding of 5FPy to the E64A mutant enzyme causes a downfield shift, indicating that the bound 5FPy remains in an unhydrated form in the complex with the mutant enzyme. $^{1}$H and $^{15}$N NMR analysis revealed *trans*-hydrogen bond D/H isotope effects on the hydrogen of the amide of Glu64, indicating that the carboxylate of Glu64 forms two hydrogen bonds with the hydrated 5FPy. ONIOM calculations showed that the wild-type yCD complex with the hydrated form of the inhibitor 1*H*-pyrimidin-2-one is more stable than the initial binding complex, and in contrast, with the E64A mutant enzyme, the hydrated inhibitor is no longer favored and the conversion has a higher activation energy, as well. The hydrated inhibitor is stabilized in the wild-type yCD by two hydrogen bonds between it and the carboxylate of Glu64 as revealed by $^{1}$H and $^{15}$N NMR analysis. To explore the functional role of Glu64 in catalysis, we investigated the deamination of cytosine catalyzed by the E64A mutant by ONIOM calculations. The results showed that without the assistance of Glu64, both proton transfers before and after the formation of the tetrahedral reaction intermediate become partially rate-limiting steps. The results of the experimental and computational studies together indicate that Glu64 plays a critical role in both the binding and the chemical transformation in the conversion of the prodrug 5FC to the anticancer drug 5-fluorouracil.

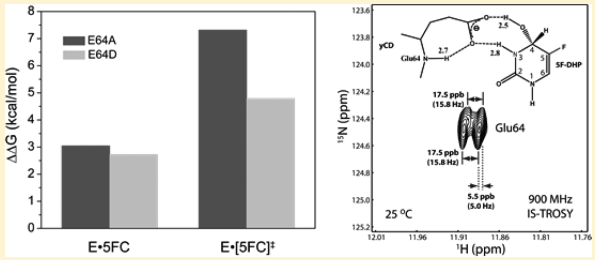


A major problem in cancer treatment is the toxicity of anticancer drugs to normal cells. Gene-directed enzyme prodrug therapy (GDEPT) is aimed at addressing this critical problem by using nontoxic prodrugs, activating them in tumors, and thereby killing cancer cells while minimizing the side effects of anticancer drugs.[1−3] One of enzyme−prodrug combinations frequently used in GDEPT is cytosine deaminase (CD) and 5-fluorocytosine (5FC). CD is a metalloenzyme that catalyzes the deamination of cytosine to generate uracil as well as the deamination of 5FC to generate 5-fluorouracil (5FU). 5FU is an anticancer drug used for the treatment of colorectal, breast, stomach, and pancreatic cancers, but like many anticancer drugs, 5FU is highly toxic, causing side effects such as myelosuppression, mucositis, dermatitis, and diarrhea. 5FC is fairly nontoxic, as CD is absent in humans. By activating the prodrug 5FC in the tumor, the CD/5FC-based GDEPT minimizes the side effects of 5FU.

Two CDs have been used as the activating enzyme in the CD/5FC-based GDEPT. One is from *Escherichia coli* (eCD) and the other from yeast (yCD). The two enzymes have no detectable homology and differ both in size and in tertiary and quaternary structures, arising apparently by convergent evolution. The *E. coli* enzyme is a homohexameric protein with a molecular mass of 47.5 kDa per subunit and has a TIM-barrel fold,[4] whereas the yeast enzyme is a homodimeric protein with a molecular mass of 17.5 kDa per subunit and has a three-layer $\alpha-\beta-\alpha$ fold.[5,6] Although eCD was used in early GDEPT studies, among wild-type CDs, yCD is preferable for GDEPT, because yCD has a much higher catalytic efficiency for 5FC than eCD.[7−9] However, a most recent study showed that a mutant form of eCD is superior to yCD.[10]

**Received:** October 4, 2011
**Revised:** November 28, 2011
**Published:** December 15, 2011

Because of its biomedical significance, there have been both experimental and computational studies of the catalytic mechanism of yCD. The structure of yCD has been determined by X-ray crystallography at high resolution, including the ligand-free form[5] and the complex form with the inhibitor 1*H*-pyrimidin-2-one (Py).[5,6] The bound Py is in the hydrated form 4(*R*)-hydroxy-3,4-dihydro-1*H*-pyrimidin-2-one (DHP), mimicking the transition state for the deamination of cytosine. The key elements of the catalytic apparatus of yCD are believed to be a bound zinc ion, which is partially coordinated by bound DHP, and a completely conserved glutamate residue, Glu64, which has two hydrogen bonds to DHP (Figure 1). The

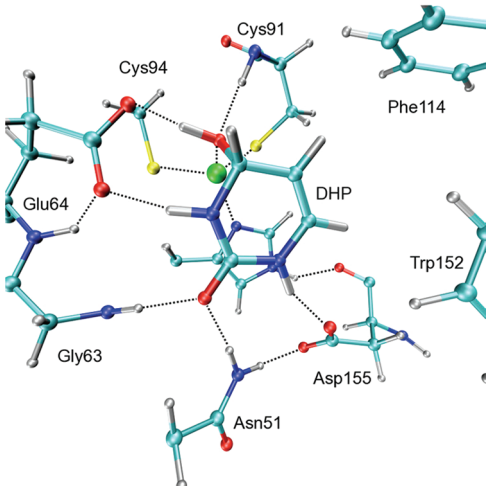


**Figure 1.** Interactions of the transition-state analogue DHP with yCD. The drawing is based on the 1.14 Å resolution crystal structure of yCD in complex with DHP (PDB entry 1P6O).[5] Hydrogen atoms were added using InsightII. The zinc atom (green) is coordinated with His62, Cys91, Cys94, and the 4-hydroxyl group of DHP.

catalytic mechanism of yCD has been investigated by both experimental and computational approaches.[11−16] Transient kinetic and NMR studies have shown that product release is rate-limiting in the activation of 5FC by yCD.[13] A complete reaction pathway for the deamination of cytosine by yCD has been proposed by two-layer quantum mechanics calculations using the ONIOM method[11] and combined molecular dynamics simulations and ONIOM calculations.[14] In the proposed reaction pathway, Glu64 plays a critical role in catalysis, serving as a proton shuttle for both the generation of the tetrahedral reaction intermediate from substrate cytosine and the conversion of the intermediate to the product uracil. However, the role of Glu64 in the enzymatic reaction has not been investigated experimentally. In this work, we have investigated the role of Glu64 in the activation of 5FC by combined experimental and computational approaches.

## EXPERIMENTAL PROCEDURES

**Materials.** Restriction enzymes and T4 ligase were purchased from New England Biolabs. *Pfu* DNA polymerase was purchased from Stratagene. [6-$^3$H]-5-Fluorocytosine was purchased from Moravek. All other chemicals and biochemicals, including cytosine, 5-fluorocytosine, and 5-fluorouracil, were purchased from Sigma-Aldrich.

**Chemical Synthesis of 5-Fluoro-1*H*-pyrimidin-2-one (5FPy).** 5FPy was synthesized via a two-step procedure. 5-Fluoro-4-thiouracil (5F4SU) was first prepared from 5FU by thiation with Lawesson's reagent in 1,4-dioxane according to a published procedure.[17] 5FPy was obtained by the Raney-Ni-catalyzed desulfurization of 5F4SU.[18] The compounds were characterized by spectrophotometry and NMR spectroscopy. All received data were in agreement with the literature.

**Cloning and Site-Directed Mutagenesis.** The plasmid construct for the overproduction of yCD with a TEV protease-cleavable N-terminal His tag was made by PCR cloning using the plasmid construct pET17b-yCD[13] as a template. The PCR primers were 5′-GGG ATC CAT ATG GCA AGC AAG TGG GAT CAG-3′ and 5′-GGA ATT CTA CTC ACC AAT ATC TTC AAA CC-3′. The PCR product was digested with *Nde*I and *Eco*RI restriction enzymes and ligated with vector pET-17bHR digested with the same restriction enzymes. The ligation mixture was transformed into *E. coli* strain DH5α. The correct coding sequence of the cloned yCD gene was verified by DNA sequencing of the entire gene. The resultant plasmid construct (pET17bHR-yCD) was then transformed into *E. coli* strain BL21(DE3) pLysS for the production of a His-tagged yCD.

The E64A mutation was made by PCR-based site-directed mutagenesis using the plasmid construct pET17b-yCD[13] as a template. The PCR primers were 5′-CC ACA CAT GGT GCG ATC TCC ACT TTG GAA AAC-3′ and 5′-GTT TTC CAA AGT GGA GAT CGC ACC ATG TAG TGT GG-3′. The mutants were selected and verified by DNA sequencing. For the production of a His-tagged E64A mutant enzyme, the mutated gene was excised with *Nde*I and *Eco*RI restriction enzymes and cloned into expression vector pET-17bHR.

The E64D mutation was made by PCR-based site-directed mutagenesis using the plasmid construct pET17bHR-yCD as a template. The PCR primers for the E64D mutagenesis were 5′-CC ACA CTA CAT GGT GAC ATC TCC ACT TTG GAA AAC-3′ and 5′-GTT TTC CAA AGT GGA GAT GTC ACC ATG TAG TGT GG-3′. The mutants were selected and verified again by DNA sequencing.

All the mutant plasmid constructs were transformed into *E. coli* strain BL21(DE3) pLysS for protein production.

**Expression and Purification.** All the nontagged proteins were produced and purified using the same protocol as previously described.[13] The His-tagged proteins were purified by chromatography on a Ni-NTA agarose column. The bacterial lysate was loaded onto the column pre-equilibrated with 10 mM imidazole in precooled buffer A [50 mM potassium phosphate buffer (pH 8.0) and 300 mM NaCl]. The column was washed with the equilibration buffer until the $OD_{280}$ of the effluent was <0.05. The column was then eluted with a linear 10 to 250 mM imidazole gradient in buffer A. Fractions containing the yCD protein were identified by SDS−PAGE and concentrated with an Amicon concentrator using a YM10 membrane. The protein solution was then subjected to TEV protease digestion for 4 h at room temperature in the presence of 0.5 mM EDTA and 1 mM DTT. The digested protein solution was dialyzed against buffer A. The His tag released by the TEV protease digestion and the undigested protein were removed by loading the dialyzed protein solution onto another Ni-NTA agarose column. The flow-through fraction was collected, concentrated, dialyzed against 2 mM phosphate buffer (pH 8.0), and lyophilized. The protein powder was kept at −80 °C until it was used.

**Kinetic Measurements.** Steady-state kinetic parameters were measured by a radiometric assay and, for E64A, also by a high-performance liquid chromatography (HPLC) assay. For


dx.doi.org/10.1021/bi201540z | *Biochemistry* 2012, 51, 475−486

both assays, the buffer contained 50 mM sodium phosphate (pH 7.5) and 50 mM NaCl. The enzyme concentrations were 1, 34, and 500 $\mu$M for wild-type yCD, E64D, and E64A, respectively. The 5FC concentration ranges were 0.08–0.68 mM for wild-type yCD, 6–64 mM for E64D, and 10–100 mM for E64A. A trace amount of [6-$^3$H]5FC was used to quantify the conversion of 5FC to 5FU. The reaction was initiated and quenched and the product 5FU separated from the substrate 5FC by TLC as previously described.[13] The reaction times were 10 s, 8 h, and 30 h for wild-type yCD, E64D, and E64A, respectively. Kinetic parameters were obtained by nonlinear least-squares fitting of the data to the standard Michaelis–Menten equation. In the HPLC assay, the reaction was quenched by the addition of an equal volume of 0.1 N HCl. The quenched solutions were injected onto a reverse-phase C18 column (22 mm × 250 mm). The column was eluted with 20 mM phosphate buffer (pH 2.0) and the elution monitored by UV absorption at 256 nm. The retention times for 5FC and 5FU were 3.6 and 5.8 min, respectively. The peak area of 5FU was integrated and compared with standard samples of known concentrations.

**Fluorometric Measurement.** The dissociation constant for the binding of 5FPy to wild-type yCD was measured by fluorometry using a FluoroMax-2 fluorometer. A series of 5FPy solutions at different concentrations were made in 50 mM phosphate buffer (pH 7.5). A yCD stock solution in the same buffer was added to these 5FPy solutions, and the mixtures were incubated at room temperature for 10 min for them to reach equilibrium. yCD and 5FPy concentrations were 1 and 0–6.4 $\mu$M, respectively. Fluorescence intensities were measured at an emission wavelength of 386 nm with a slit width of 4 nm. The excitation wavelength and slit width were 320 and 4 nm, respectively. A set of controls was obtained in the same manner by adding the buffer instead of the protein stock solution. The $K_d$ value was obtained by nonlinear least-squares fitting of the difference data to the following equation based on an independent one-on-one (one ligand per subunit) binding model:

$$\Delta F = \left\{ df\left[ P_t + L_t + K_d - \sqrt{(P_t + L_t + K_d)^2 - 4P_tL_t} \right] \right\}/(2P_t)$$

where $\Delta F$ is the fluorescence change upon ligand binding, $df$ is the fluorescence intensity difference per unit concentration between the bound and free form of 5FPy, $P_t$ and $L_t$ are the total concentrations of the enzyme and 5FPy, respectively, and $K_d$ is the dissociation constant of 5FPy with the yCD enzyme.

**Inhibition Assay.** The inhibition of the 5FC deamination reaction by 5FPy was measured by the radiometric assay as described earlier. $IC_{50}$ values were obtained by nonlinear least-squares fitting of the inhibition assay data to the following equation:

$$v = k_{min} + \frac{k_{max} - k_{min}}{1 + \frac{[I]}{IC_{50}}}$$

where $v$ is the initial reaction rate, $k_{min}$ the minimum rate, $k_{max}$ the maximum rate, and [I] the concentration of the inhibitor. $K_i$ values were calculated by the Cheng–Prusoff equation:[19]

$$K_i = \frac{IC_{50}}{1 + \frac{[S]}{K_m}}$$

where [S] is the concentration of the substrate 5FC.

**$^{19}$F NMR Spectroscopy.** NMR samples were prepared by dissolving wild-type yCD or the E64A mutant enzyme in 100 mM potassium phosphate buffer (pH 7.5) made in $D_2O$. An aliquot of a 5FPy stock solution was added to the protein solutions, and the mixtures were incubated for 10 min to reach equilibrium. $^{19}$F NMR experiments were performed at 10 or 20 °C on a Varian Inova 600 MHz NMR spectrometer. NMR spectra were acquired with a spectral width of 10000 Hz, 20000 complex data points, and 1024 transients and processed with a 10 Hz line broadening. The relaxation delay was 6 s. The $^{19}$F chemical shifts were referenced to $CF_3C_6H_5$, which was set to −63.73 ppm.

**$^1$H and $^{15}$N NMR Spectroscopy.** The $^{15}$N–$^1$H ISTROSY[20,21] spectrum was recorded at 25 °C on a Bruker AVANCE 900 MHz NMR spectrometer equipped with a TCI cryoprobe using a sample of $^2$H-, $^{13}$C-, and $^{15}$N-labeled yCD in complex with 5FPy in the 1:1 $D_2O/H_2O$ buffer. The sample was prepared as previously described.[13] Standard jump–return $^1$H spectra of apo yCD and the 5FPy complexes of the wild-type and the E64A mutant enzyme were recorded on a Varian INOVA 600 MHz NMR spectrometer with an HCN triple-resonance probehead at either 10 or 25 °C.

**ONIOM Calculations.** A two-layer ONIOM method[22−29] as implemented in Gaussian 03[30] was used to investigate the effects of the E64A mutation on yCD catalysis. The molecular setup and protocol for the ONIOM calculations were essentially the same as those previously described.[11] Briefly, the molecular system for the calculations was based on the 1.14 Å resolution crystal structure of the yCD·DHP complex (PDB entry 1P6O).[5] The enzyme was modeled by the catalytic Zn and the active site and neighboring residues, including Ile33, Asn51, Thr60, Leu61, His62, Gly63, Glu64, Ile65, Leu88, Ser89, Pro90, Cys91, Asp92, Met93, Cys94, Thr95, Phe114, Trp152, Phe153, Glu154, Asp155, and Ile156.[11,12,14,15] The system was divided into two layers. The inner layer was composed of the side chains of residues Glu64, His62, Cys91, Cys94, Asn51, and Asp155, the zinc ion, the zinc-bound water, and cytosine or Py. The rest of the molecular system constituted the outer layer. Hydrogen atoms were used as link atoms to saturate the dangling bonds. The inner layer was treated with the B3LYP density functional method[31,32] employing the 6-31G** basis set and the outer layer by the semiempirical PM3 method.[33,34] The total ONIOM energy ($E^{ONIOM}$) is given by[22,23]

$$E^{ONIOM} = E(\text{high,model}) + E(\text{low,real}) - E(\text{low,model})$$

where $E$(high,model) and $E$(low,model) are the energies of the inner layer at the high level of theory (B3LYP and the 6-31G** basis set) and at the low level of theory (PM3), respectively, and $E$(low,real) is the energy of the entire system at the PM3 level.


dx.doi.org/10.1021/bi201540z | Biochemistry 2012, 51, 475–486

## RESULTS

**Biochemical Analysis.** To investigate the role of Glu64 in the activation of the anticancer prodrug 5FC, we replaced Glu64 with alanine and aspartate. Preliminary biochemical characterization of the mutant enzymes without a His tag indicated that the purified mutant enzymes contained a minute amount of eCD, resulting in steady-state kinetic curves requiring two $K_m$ values to fit the data, although the *E. coli* enzyme is not homologous to the yeast enzyme, different in both size and quaternary structure. To eliminate the eCD contamination, both wild-type yCD and mutants were subcloned into a vector for the production of His-tagged proteins. The His-tagged proteins were purified with two Ni-NTA agarose columns. In the first column, proteins bound to Ni-NTA were eluted and collected. The protein solution was then subjected to TEV protease digestion to remove the N-terminal His tag from the tagged yCD. The TEV protease-digested protein solution was loaded onto the second Ni-NTA agarose column, in which the flow-through was collected. The second column removed not only undigested yCD but also proteins copurified with yCD by the first Ni-NTA agarose column. The kinetic behavior of such a yCD mutant enzyme preparation was normal, i.e., requiring only one $K_m$ to fit the kinetic data. The protein was purified further by gel filtration (Sephadex G-75) in trial experiments, but the kinetic properties of the protein purified by the three-column procedure were the same as those of the protein purified by the two-column procedure, indicating that the purification procedure with two Ni-NTA columns was effective in removing eCD.

Our analysis was focused on the effects of the E64A mutation, because the mutation completely removed the carboxyl functional group. The steady-state kinetic parameters of wild-type (WT) yCD and mutant enzymes E64A and E64D are summarized in Table 1. Because of the relatively large errors of the radiometric assay in measuring a small amount of 5FU in the presence of a large amount of 5FC, the kinetic parameters of the E64A mutant enzyme were also determined by an HPLC assay. Both mutations caused a dramatic decrease in $k_{cat}$ and a dramatic increase in $K_m$ (Table 1). The E64A mutation caused a decrease in $k_{cat}$ of ~5 orders of magnitude and an increase in $K_m$ of ~2 orders of magnitude, resulting in a decrease in $k_{cat}/K_m$ of ~8 orders of magnitude. The effects of the E64D mutation were only slightly milder. The kinetic results indicated that Glu64 is involved in both binding and catalysis in the activation of 5FC by yCD, and the longer side chain is important, as Glu64 cannot be replaced with aspartate with the same functional group but a shorter side chain.

**Table 1. Kinetic Constants of Wild-Type yCD and the E64 Mutant Enzymes for the Activation of 5FC**

| protein | $K_m$ (mM) | $k_{cat}$ ($s^{-1}$) | $k_{cat}/K_m$ ($mM^{-1}$ $s^{-1}$) |
|---|---|---|---|
| WT yCD | 0.16 ± 0.01 | 17 ± 0.4 | 106 |
| E64A | 89 ± 30[a] | (1.3 ± 0.3) × $10^{-4}$[a] | 1.4 × $10^{-6}$[a] |
| | 33 ± 6[b] | (7.3 ± 0.6) × $10^{-5}$[b] | 2.2 × $10^{-6}$[b] |
| E64D | 19 ± 6 | (5.1 ± 1.0) × $10^{-3}$ | 2.6 × $10^{-4}$ |

[a]Determined by a radiometric assay. [b]Determined by an HPLC assay.

To further investigate the role of Glu64 in the activation of 5FC, we measured the binding and inhibitory activities of the putative transition-state analogue 5FPy. The results are summarized in Table 2. The inhibitory activity of yCD was measured for the E64D mutant enzyme but not for E64A, because the activity of the latter was too low for such an analysis. The E64D mutation caused a decrease in $K_i$ of ~4 orders of magnitude, indicating that the mutant enzyme has a much lower affinity for 5FPy than wild-type yCD. The $K_d$ value for the binding of 5FPy could be measured by fluorometric titration for wild-type yCD but not for either of the two mutant enzymes, because the method is not suitable for the weak binding of 5FPy to the mutant enzymes. The $K_d$ value for the binding of 5FPy to the E64A mutant enzyme was estimated by NMR as described below.

**Table 2. Inhibitory and Binding Properties of 5FPy**

| protein | $K_i$ (μM) | $K_d$ (μM) |
|---|---|---|
| WT yCD | 0.86 ± 0.16 | 0.65 ± 0.08[a] |
| E64A | | 1.0 × $10^{4}$[b] |
| E64D | 1060 ± 60 | |

[a]Measured by fluorometric titration. [b]Estimated by $^{19}$F NMR.

**$^{19}$F NMR Analysis.** The bound Py in the crystal structure of yCD is in the hydrated form DHP.[5,6] 5FPy differs from Py in having a fluorine atom at position 5 instead of a hydrogen atom. To determine whether the bound 5FPy is hydrated like Py and the role of Glu64 in the hydration, $^{19}$F NMR spectra were acquired for 5FPy in the absence or presence of yCD (the wild-type or E64A mutant enzyme) (Figure 2). In the absence of the enzymes, 5FPy showed a sharp peak at −160.6 ppm. In the presence of a lower concentration of wild-type yCD, 5FPy showed an additional broad peak due to the bound 5FPy around −161.1 ppm, upfield of the peak of free 5FPy. In the presence of the same concentration of the E64A mutant enzyme, 5FPy also showed a broad but much smaller peak due to the bound 5FPy at −158.1 ppm, downfield from the peak of free 5FPy. Using model compounds, it has been shown that the

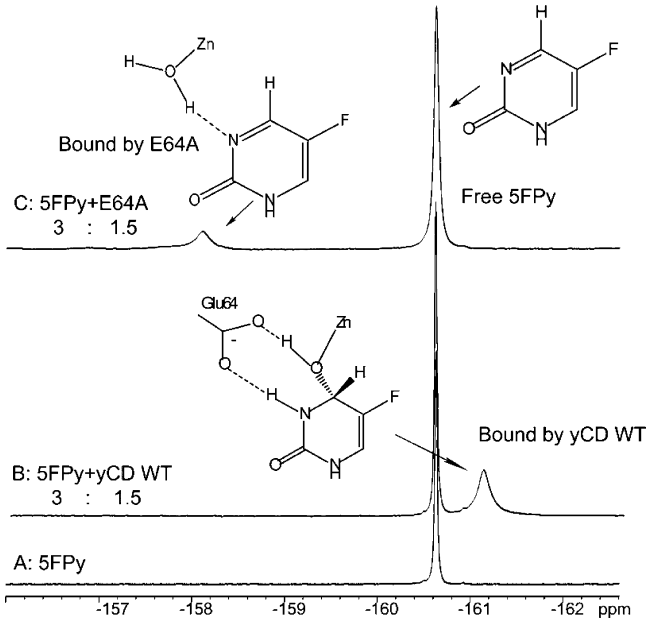


**Figure 2.** $^{19}$F NMR spectra of the wild-type yCD−5FPy complex and the E64A−5FPy complex. All samples were in a $D_2O$ buffer containing 100 mM potassium phosphate (pH 7.5). (A) Spectrum of 5FPy (4.0 mM) in the absence of wild-type yCD or E64A. (B) Spectrum of 5FPy (3.0 mM) in the presence of wild-type yCD (1.5 mM). (C) Spectrum of 5FPy (3.0 mM) in the presence of E64A (1.5 mM).


dx.doi.org/10.1021/bi201540z | *Biochemistry* 2012, 51, 475−486

$^{19}$F NMR signal is a good indicator of the hydration of 5FPy.[35] The hydration of 5FPy results in a change in the bonding of C4 from sp$^2$ to sp$^3$, causing an ~1 ppm upfield shift of the $^{19}$F NMR signal. This upfield shift of the $^{19}$F NMR signal has been used for the determination of the hydration state of 5-fluoropyrimidin-2-one ribonucleoside.[35] The dramatic opposite shift of the $^{19}$F NMR signal of 5FPy indicated that 5FPy is hydrated when it binds to wild-type yCD and is not hydrated when it binds to the E64A mutant enzyme. In either case, however, free 5FPy is in slow exchange with the bound 5FPy on the NMR chemical shift time scale. In such an exchange regime, the chemical shift does not change with protein or ligand concentration and cannot be used for the estimation of $K_d$ values. However, the relative peak intensities of the NMR signals of the free form and the bound form can be used to estimate the $K_d$ value if the protein and ligand concentrations are on the same order of magnitude as the $K_d$ value. The protein and 5FPy concentrations were suitable for the estimation of the $K_d$ value for the E64A mutant enzyme but not for wild-type yCD. The $K_d$ value for the binding of 5FPy to the E64A mutant enzyme was estimated to be ~10 mM on the basis of the $^{19}$F NMR data, ~5 orders of magnitude higher than that for the binding of 5FPy to the wild-type enzyme. As 5FPy is the hydrated form when it binds to wild-type yCD and the unhydrated form is favored over the hydrated form by a factor of $2.9 \times 10^3$, the $K_d$ for the binding of hydrated 5FPy, a transition-state analogue, to wild-type CD was estimated to be $2.3 \times 10^{-10}$ M.

**$^1$H and $^{15}$N NMR Analysis.** In the crystal structures of the yCD·DHP complex,[5] one of the Glu64 side chain carboxyl oxygen atoms, O$^{\varepsilon 2}$, forms a strong H-bond to the O4 H moiety of the hydrated inhibitor with a distance of ~2.5 Å between the two oxygen atoms, and the other carboxyl oxygen, O$^{\varepsilon 1}$, forms a normal H-bond with the N3 H imino group of the ligand. O$^{\varepsilon 1}$ is also bifurcatedly H-bonded to the backbone amide of the same residue (Figures 1 and 3). Because the bound 5FPy is in the hydrated form (5F-DHP) as indicated by the $^{19}$F NMR analysis, we investigated the H-bonding of Glu64 in the yCD·5F-DHP complex by $^1$H and $^{15}$N NMR. Shown in Figure 3 is a close-up view of the Glu64 backbone amide resonance in the $^{15}$N−$^1$H IS-TROSY[20,21] spectrum of the yCD·5F-DHP complex. The resonance clearly shows a doublet with a splitting of 17.5 ppb (15.8 Hz at the 900 MHz field for $^1$H) due to the *trans*-H-bond D/H isotope effect[36,37] on the N3 H imino hydrogen of the ligand transmitted via O$^{\varepsilon 1}$, because the corresponding resonance with a similar sample in water leads to a singlet. The large *trans*-H-bond D/H isotope effect indicates that the O$^{\varepsilon 1}$-mediated bifurcated H-bonds are strong.[36,37] Interestingly, a closer inspection on the doublet reveals that it is actually a partial overlap from two sets of doublets with the upper set (upfield in the $^{15}$N dimension) having a 5.5 ppb (5.0 Hz at a 900 MHz field) upfield shift in the $^1$H dimension with respect to the lower set (downfield in the $^{15}$N dimension). Because no other exchangeable protons are in the vicinity of the Glu64 backbone amide, the 5.5 ppb shift difference must be a consequence of the D/H isotope effect on the O4 H of the hydrated inhibitor transmitted through the two carboxyl oxygen atoms and two H-bonds. Therefore, the observed long-range *trans*-H-bond D/H isotope effect convincingly indicates that the O$^{\varepsilon 2}$···H···O4 bond is truly a strong H-bond. This is corroborated by a 16.2 ppm peak in the jump−return $^1$H spectrum recorded at room temperature, which was assigned to the resonance of the bridging proton, because it disappeared when either the apoprotein or the E64A mutant enzyme was used in complex with 5F-DHP (Figure S1 of the Supporting Information). This chemical shift is consistent with those of protons involved in low-barrier H-bonds (LBHBs).[38] There is no other H-bond with a distance between the two heteroatoms of <2.60 Å in the yCD crystal structures.[5] On the other hand, the O4 atom of 5F-DHP is unlikely completely deprotonated by Glu64; otherwise, the observed long-range *trans*-H-bond D/H isotope effect would be much larger. Because the O$^{\varepsilon 1}$-mediated H-bonds are strong as indicated by the 17.5 ppb *trans*-H-bond D/H isotope effect, D/H isotope effects through four covalent bonds can be up to 150 ppb as observed at the active site histidine imidazole ring of the bovine pancreatic enzyme sPLA$_2$ in complex with a phosphonate transition-state analogue.[40]

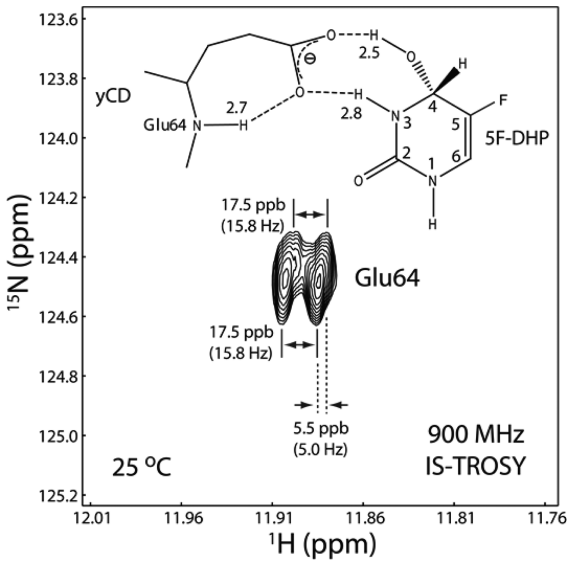


**Figure 3.** Region of the $^{15}$N−$^1$H IS-TROSY spectrum of the Glu64 backbone amide resonance. The inset is the schematic diagram of hydrogen bonding between yCD and 5F-DHP derived from the 1.14 Å resolution crystal structure (PDB entry 1P6O).[5] Lengths (angstroms) of H-bonds are indicated.

**Computational Analysis.** Because 5FPy is hydrated when bound to wild-type yCD but not hydrated when bound to the E64A mutant enzyme, we investigated the hydration by yCD by ONIOM calculations taking advantage of the availability of the high-resolution crystal structure of the enzyme in complex with DHP, the hydrated form of Py. Py was docked in the active site by superposition with DHP in the X-ray crystal structure.[5] After optimization, Py shifted slightly from the initial position to give complex **1** (Figures 4 and 5). Complex **1** is stabilized through a H-bond network and a $\pi$-stacking interaction. One new interaction is presented between the zinc-coordinated water O$^{Zn}$ and N3 of Py. Glu64 is in the deprotonated form and forms a strong H-bond with the other hydrogen of the zinc-coordinated water. The carbonyl oxygen (O2) of Py is H-bonded to the side chain amide of Asn51 and the backbone amide of Gly63. The amide group at position 1 (N1) of Py is H-bonded to the carboxyl group of Asp155. The latter is also H-bonded to the side chain amide of Asn51. The H-bond between the amide group (N$^{\varepsilon 2}$) of His62 and the backbone carbonyl oxygen (O$^{\delta 1}$) of Asp155 helps in maintaining the appropriate orientation of the imidazole ring of His62 that stacks with the cytosine ring. Before the hydration occurs, the


dx.doi.org/10.1021/bi201540z | *Biochemistry* 2012, 51, 475−486

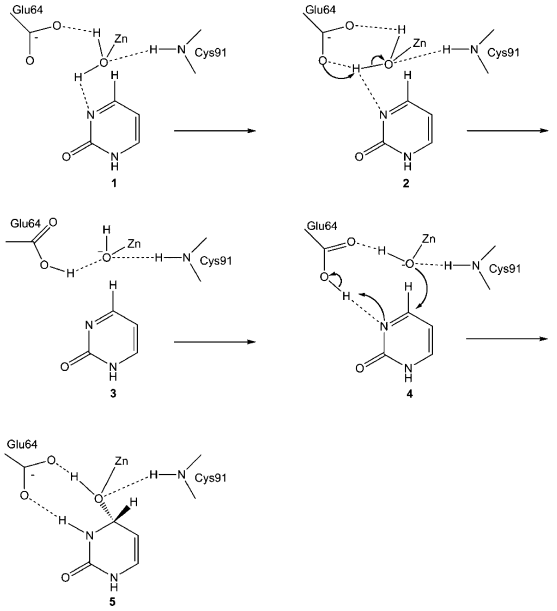


**Figure 4.** Proposed reaction pathway from Py to DHP catalyzed by wild-type yCD. The proposed reaction intermediates are based on the ONIOM calculations as illustrated in Figure 5.

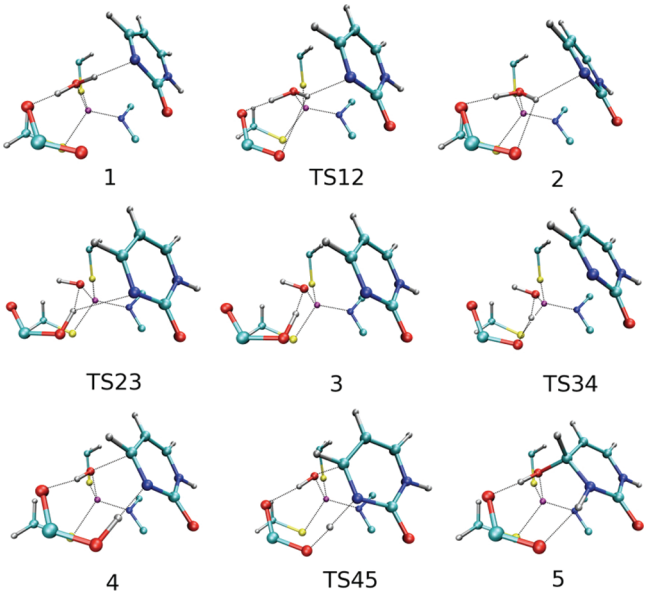


**Figure 5.** ONIOM-optimized structures for the conversion of Py to DHP by wild-type yCD: complex **1**, **TS12** between complexes **1** and **2**, complex **2**, **TS23** between complexes **2** and **3**, complex **3**, **TS34** between complexes **3** and **4**, complex **4**, **TS45** between complexes **4** and **5**, and complex **5**.

water is converted to a hydroxide with the assistance of Glu64. First, the H-bond between $O^{Zn}$ and N3 is broken and a new H-bond between $O^{Zn}$ and Glu64 is formed (not the one already presented). The new conformation is given in complex **2** (Figures 4 and 5). In this complex, the $O^{Zn}$···N3 H-bond is not completely disrupted. One important feature of this conformation is that the distance between $O^{Zn}$ and C4 is shortened because the change in the position of $H^{OZn}$ reduces the steric hindrance. Complex **2** is calculated to be less stable than **1** by 2.9 kcal/mol (Figure 6). However, **2** is more stable than **1** by 5.4 kcal/mol at the *E*(high,model) energy level. The difference

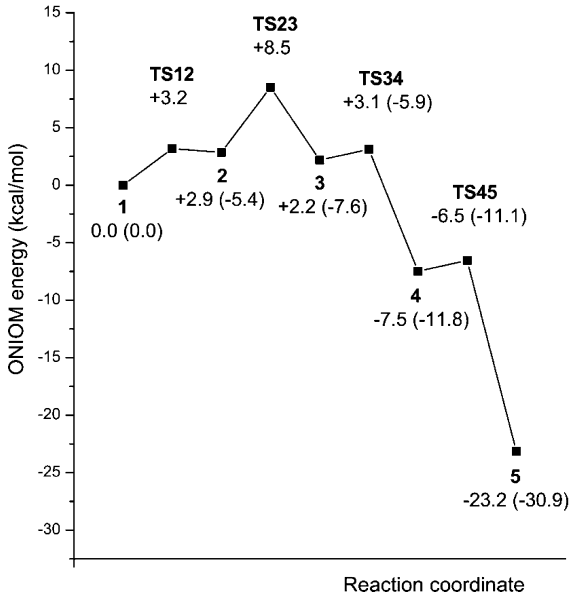


**Figure 6.** Schematic $E^{ONIOM}$ and *E*(high,model) energy profile for the conversion of Py to DHP catalyzed by wild-type yCD.

of 8.3 kcal/mol indicates the surrounding residues destabilize the complex. The corresponding barrier is 3.2 kcal/mol, and there is no barrier found at the *E*(high,model) energy surface. Second, $H^{OZn}$ is transferred from $O^{Zn}$ to Glu64, as seen in complex **3** (Figures 4 and 5). In this process, the H-bond between $O^{Zn}$ and N3 is completely broken. After the proton transfer, a strong H-bond is formed between the Zn-coordinated hydroxide and the OH group of Glu64. The distance between $O^{Zn}$ and C4 is further reduced. Complex **3** is slightly more stable than complex **2**. The energy barrier is calculated to be 5.6 kcal/mol at the ONIOM energy level. Again, there is no barrier found at the *E*(high,model) level. In the next step, the H-bond between $O^{Zn}$ and the OH group of Glu64 is broken and a new H-bond is formed between the OH group of Glu64 and N3, which can be seen in complex **4** (Figures 4 and 5). The distance between $O^{Zn}$ and C4 is shortened to 2.17 Å. The energy barrier is 0.9 kcal/mol at the ONIOM energy level and 1.7 at the *E*(high,model) energy level. Complex **4** is more stable than the initial complex **1** by 7.5 kcal/mol at the ONIOM energy level and by 11.8 kcal/mol at the *E*(high,model) energy level. The Zn-coordinated hydroxide in complex **4** is well positioned for the nucleophilic attack on C4. The distance between the hydroxide and C4 decreases from 3.01 Å in complex **1** to 2.66 Å in complex **2**, to 2.44 Å in complex **3**, and to 2.17 Å in complex **4**. The nucleophilic attack on C4 is concomitant with the transfer of a proton from the OH group of Glu64 to N3, resulting in the formation of the tetrahedral product (DHP) as shown in complex **5** (Figures 4 and 5). The energy barrier is 1.0 kcal/mol at the ONIOM level and 0.7 kcal/mol at the *E*(high,model) level. The bond lengths, bond angles, and dihedral angles of DHP in complex **5** are in close agreement with those of DHP in the crystal structure (Table 3). The yCD−DHP complex is more stable than the initial yCD·Py complex by 23.2 kcal/mol at the ONIOM level and 30.9 kcal/mol at the *E*(high,model) level. The difference of 7.7 kcal/mol indicates that the model system is relatively destabilized by the outer layer. **5** is considerably more stable than **1** because of the intrinsic stability of the model system, which suggests that the tight binding of the inhibitor is


dx.doi.org/10.1021/bi201540z | *Biochemistry* 2012, 51, 475−486

**Table 3. Comparison of the ONIOM-Optimized Structure of Tetrahedral Product 5 with the Crystal Structure of the yCD−Inhibitor Complex[a]**

| internal coordinate | ONIOM | X-ray structure |
|---|---|---|
| DHP O4···Zn | 2.047 | 2.066 |
| His62 $N^{\delta 1}$···Zn | 2.007 | 1.991 |
| Cys91 $S^{\gamma}$···Zn | 2.379 | 2.302 |
| Cys94 $S^{\gamma}$···Zn | 2.337 | 2.266 |
| DHP O4···DHP C4 | 1.449 | 1.475 |
| DHP N3···DHP C4 | 1.444 | 1.446 |
| $\angle S^{\gamma\ Cys91}$–Zn–$S^{\gamma\ Cys94}$ | 115.1 | 117.1 |
| $\angle N^{\delta 1\ His62}$–Zn–$S^{\gamma\ Cys91}$ | 98.4 | 102.0 |
| $\angle N^{\delta 1\ His62}$–Zn–$S^{\gamma\ Cys94}$ | 112.0 | 113.6 |
| $\angle S^{\gamma\ Cys91}$–Zn–O4 | 109.5 | 108.3 |
| $\angle S^{\gamma\ Cys94}$–Zn–O4 | 104.1 | 103.0 |
| $\angle N^{\delta 1\ His62}$–Zn–O4 | 118.2 | 113.1 |
| ∠O4–C4–C5–C6 | 112.6 | 113.1 |
| ∠O4–C4–N3–C2 | 110.8 | 114.4 |

[a]Bond distances in angstroms and angles in degrees.

mainly due to the high affinity of DHP for wild-type yCD. The results of the calculations using Gaussian 09 on the conversion of Py to DHP and 5FPy to 5F-DHP are similar (data not shown).

To investigate the effects of the E64A mutation on hydration, an E64A−Py complex was constructed in the same manner as the wild-type yCD complex with Py (complex **6** in Figures 7

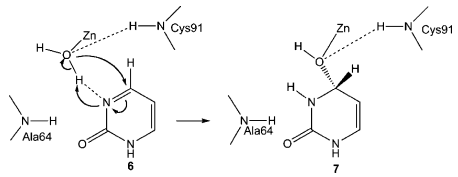


**Figure 7.** Proposed reaction pathway from Py to DHP catalyzed by the E64A mutant enzyme.

and 8), assuming that the structure of the E64A mutant enzyme is the same as that of wild-type yCD. The conformation of the optimized complex **6** is similar to that of the corresponding wild-type yCD complex. The Zn-coordinated water, however, forms only one H-bond (with N3 of Py), and the other H-bond in the yCD·Py complex is absent, as Glu64 is not present in the mutant enzyme complex. Because of the lack of Glu64, the Zn-coordinated water cannot be converted to hydroxide before the nucleophilic attack on C4. The distance between $O^{Zn}$ and C4 is 3.08 Å, longer than that in the yCD·Py complex, making it even harder to attack C4. The nucleophilic attack of the Zn-coordinated water on C4 of Py is concomitant with the transfer of one of its protons to N3 of Py to form the tetrahedral product as in complex **7** (Figures 7 and 8). The approximate geometry of transition state **TS67** was found by scanning the $H^{OZn}$–N3 and $O^{Zn}$–C4 distances from complex **6** to complex **7**. The transition state was found to have an $O^{Zn}$–C4 distance of 2.58 Å. The energy barrier is 14.4 kcal/mol at the ONIOM energy level and 36.1 kcal/mol at the *E*(high,model) level (Figures 7–9), indicating that the protein environment (the

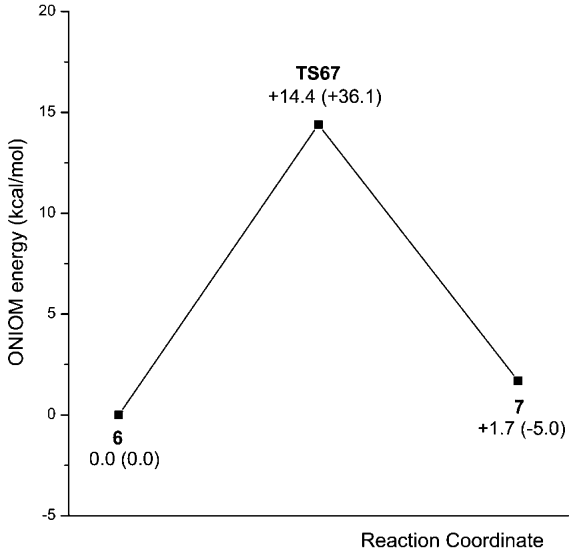


**Figure 9.** Schematic $E^{ONIOM}$ and *E*(high,model) energy profile for the conversion from Py to DHP catalyzed by the E64A mutant enzyme.

outer layer) compensates for the barrier by 21.7 kcal/mol. The energy barrier is much higher than the corresponding energy barrier in the hydration catalyzed by wild-type yCD. It is noted that the proton is transferred slightly ahead of the formation of the $O^{Zn}$–C4 bond. Complex **7** is calculated to be less stable than **6** by 1.7 kcal/mol at the ONIOM level, indicating that the unhydrated form is favored in the active center of the yCD E64A mutant enzyme.

To investigate further the effects of the E64A mutation on the deamination reaction, a complex of the E64A mutant enzyme with the substrate cytosine was constructed as for the construction of the wild-type enzyme−substrate complex,[11] assuming again that the structure of the mutant enzyme is the same as that of the wild-type enzyme. A water molecule was added in place of the carboxyl group of Glu64. After optimization, cytosine shifted slightly from the initial position to give complex **8** (Figures 10 and 11). The interactions between the substrate and enzyme in complex **8** are similar to those in the corresponding wild-type enzyme complex,[11] except the interaction involving the Zn-coordinated water and Glu64. In the wild-type enzyme complex, Glu64 forms a H-bond with

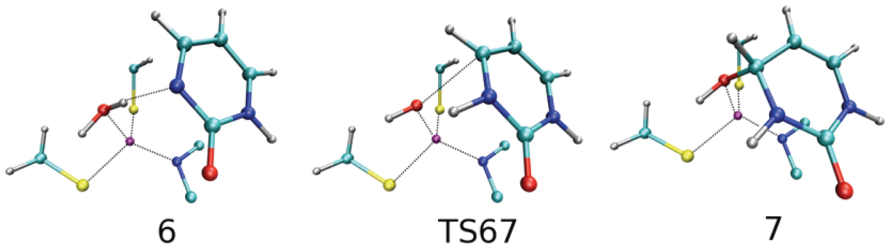


**Figure 8.** ONIOM-optimized structures for the conversion of Py to DHP by the E64A mutant enzyme: complex **6**, **TS67** between complexes **6** and 7, and complex 7.


dx.doi.org/10.1021/bi201540z | *Biochemistry* 2012, 51, 475−486

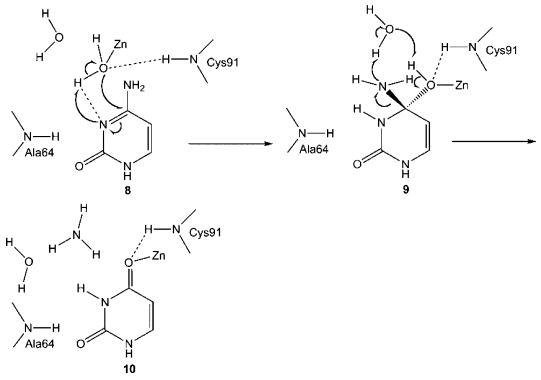


**Figure 10.** Conversion of cytosine to the zinc-coordinated uracil catalyzed by the E64A mutant enzyme.

the Zn-coordinated water and another with the amino group of cytosine. In the mutant enzyme complex, the Zn-coordinated water forms a H-bond with N3 of cytosine, and the amino group of cytosine forms a H-bond with the additional water molecule. As the Zn-coordinated water is H-bonded to N3 and cannot be deprotonated by the additional water molecule, the Zn-coordinated hydroxyl is generated by the direct transfer of a proton to N3, but the hydroxide is not as well positioned for the nucleophilic attack on C4 as in the corresponding wild-type complex.[11] The distance between $O^{Zn}$ and C4 is only 2.24 Å in the wild-type enzyme complex but is 2.9 Å in the mutant enzyme complex. The transition state is found when the distance between $O^{Zn}$ and C4 is 2.48 Å. The energy barrier for the nucleophilic attack is calculated to be 11.2 kcal/mol at the ONIOM energy level and 22.1 kcal/mol at the *E*(high,model) level (Figure 12). For the wild-type yCD-catalyzed reaction, the formation of the tetrahedral intermediate occurs through three steps, in which the highest energy barrier is only 1.9 kcal/mol.[11] The stabilization of the tetrahedral intermediate is also affected, because the energy level of the tetrahedral intermediate is

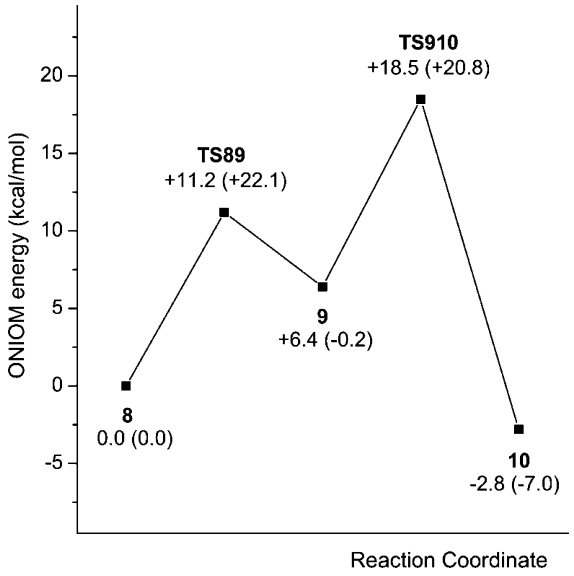


**Figure 12.** Schematic $E^{ONIOM}$ and *E*(high,model) energy profile for the conversion from cytosine to uracil catalyzed by the E64A mutant enzyme.

6.4 kcal/mol higher than that of the substrate complex in the mutant enzyme-catalyzed reaction (Figure 12). However, the energy level of the same intermediate is 10.8 kcal/mol lower than that of the substrate complex during the reaction catalyzed by wild-type yCD.[11]

Once the tetrahedral intermediate is formed, the transfer of another proton from $O^{Zn}$ to N4 is needed before the C4−N4 bond is cleaved.[11] Two possible pathways were explored. In pathway 1, the proton is transferred directly to N4 via a four-membered ring transition state. In pathway 2, the proton transfer is mediated by the additional water molecule. The water donates a proton to N4 and extracts a proton from $O^{Zn}$ in

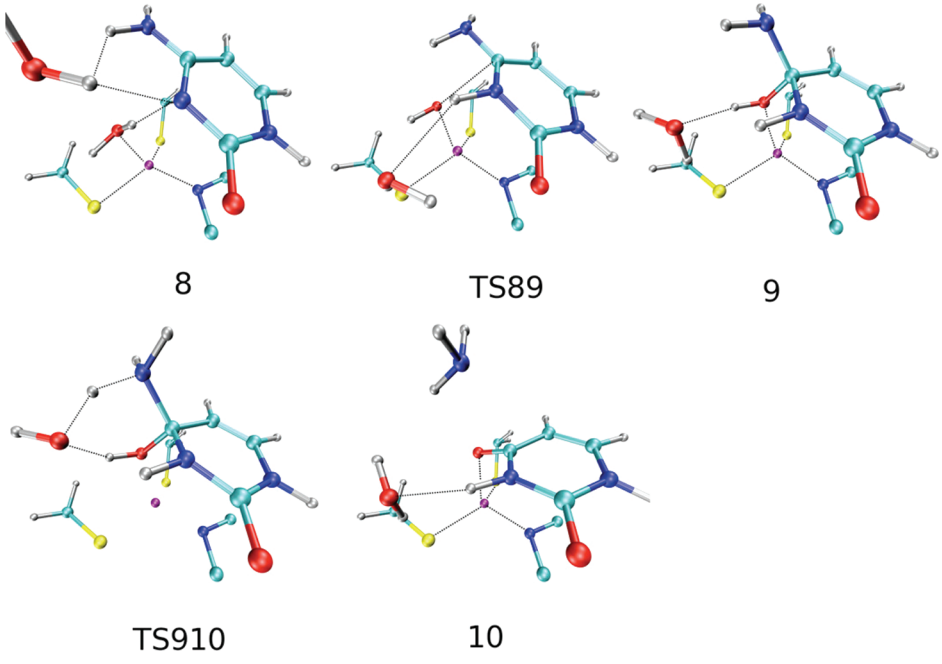


**Figure 11.** ONIOM-optimized structures for the conversion from cytosine to the zinc-coordinated uracil: complex **8**, **TS89** between complexes **8** and **9**, complex **9**, **TS910** between complexes **9** and **10**, and complex **10**.


dx.doi.org/10.1021/bi201540z | *Biochemistry* 2012, 51, 475−486

a concerted manner. The C4−N4 bond distance increases to 1.64 Å after the proton is transferred to N4. The energy barrier in the second pathway (12.1 kcal/mol at the ONIOM energy level) is dramatically lower than that in the first pathway (22.3 kcal/mol at the ONIOM energy level), indicating that the $O^{Zn}$ proton is transferred to N4 via the second pathway. The energy barrier is high when compared with that of the deamination catalyzed by wild-type yCD, in which the energy barrier is only 7.1 kcal/mol at the ONIOM energy level.[11]

## DISCUSSION

The results of the combined experimental and computational studies reported here indicate that Glu64 is important for both binding and chemical steps in the activation of the anticancer prodrug 5FC. Assuming that the activation of 5FC follows a mechanism similar to that of the deamination of cytosine, it involves the generation of a tetrahedral reaction intermediate from the substrate and the conversion of the intermediate to the product.[11] A critical role of Glu64 in the chemical steps is supported by the results of the biochemical analysis of the mutant enzymes. First, the $k_{cat}$ of the E64A mutant enzyme decreases by 5 orders of magnitude relative to that of wild-type yCD. Our previous transient kinetic and NMR studies showed that product release is rate-limiting in the activation of 5FC by wild-type yCD.[13] Consequently, the $k_{cat}$ of the wild-type enzyme is significantly smaller than the rate constant for the chemical transformation. On the other hand, the rate-limiting step is most likely the chemical transformation in the activation of 5FC by the mutant enzyme, because of its severely impaired catalytic apparatus. Therefore, the $k_{cat}$ of the E64A mutant enzyme should be compared with the corresponding rate constant of wild-type yCD for the chemical transformation, and thus, the E64A mutation decelerates the chemical transformation by 6 orders of magnitude. Glu64 contributes to the stabilization of the transition state of the activation of 5FC by ∼9 kcal/mol. Second, inhibition and binding studies indicate that the $K_i$ of the putative transition-state analogue 5FPy for the inhibition of the E64D mutant enzyme increases by 3 orders of magnitude relative to that for the inhibition of wild-type yCD, and the $K_d$ of 5FPy for the binding of the E64A mutant enzyme increases by 4 orders of magnitude relative to that for the binding of wild-type yCD, corresponding to ∼6 kcal/mol.

A more precise role of Glu64 in the activation of 5FC is revealed by the NMR analysis of the binding of 5FPy to the wild-type and mutant enzymes and the computational analysis of the hydration of Py by wild-type yCD and the deamination of cytosine by the E64A mutant enzyme. The $^{19}F$ NMR analysis shows that 5FPy is hydrated when bound to wild-type yCD but is unhydrated when bound to the E64A mutant enzyme (Figure 2), suggesting that Glu64 plays a critical role in the formation and/or stabilization of the hydrated 5FPy. The ONIOM calculations of the hydration of Py indicate that Glu64 functions as a proton shuttle for the transfer of a proton from the Zn-coordinated water to N3 of Py, and the hydration follows a sequential mechanism with N3 protonated first followed by the nucleophilic attack of C4 by the Zn-coordinated hydroxide (Figures 4−6). Furthermore, the complex of the hydrated Py is much more stable than that of the unhydrated Py, based on the dramatic difference in the ONIOM energies of the two complexes (−23.2 kcal/mol). Without the proton shuttle Glu64 in the E64A mutant enzyme, the hydration follows a concerted mechanism with a significantly higher energy barrier (14.4 kcal/mol) and the ONIOM energy of the complex of the hydrated Py is higher than that of the complex of the unhydrated Py (1.7 kcal/mol) (Figures 7−9). The results of the ONIOM calculations suggest that Glu64 both facilitates the hydration of Py and stabilizes the hydrated Py. Because the energy barrier for the hydration of the inhibitor by the E64A mutant enzyme is not insurmountable, the thermodynamic effect is more important. According to the ONIOM calculations, the carboxylate of Glu64 stabilizes the hydrated form of the inhibitor by ∼25 kcal/mol. The $^{15}N-^{1}H$ IS-TROSY analysis (Figure 3) shows that the carboxylate of Glu64 forms two H-bonds with the bound 5F-DHP, just as in the crystal structure of the yCD·DHP complex.[5,6] The two H-bonds must play a major role in the stabilization of the hydrated form of the inhibitor, because 5FPy is predominantly in the unhydrated form when bound to E64A, based on the $^{19}F$ NMR analysis. As the hydration reaction mimics the formation of the reaction intermediate in the deamination reaction, Glu64 may play a major role in the formation and stabilization of the reaction intermediate in the activation of the anticancer prodrug 5FC.

The ONIOM calculations of the deamination reaction catalyzed by the E64A mutant enzyme show that Glu64 is important for both the formation of the tetrahedral reaction intermediate from the substrate and the conversion of the reaction intermediate to the product (Figures 10−12). Without Glu64 shuttling protons, the barriers for both the formation of the tetrahedral reaction intermediate and its conversion to the product are much higher than those in the wild-type enzyme reaction. Furthermore, the ONIOM energy of the reaction intermediate complex is 10.8 kcal/mol lower than that of the substrate complex in the wild-type enzyme reaction[11] but is 6.4 kcal/mol higher in the mutant enzyme reaction (Figure 12). The combination of these effects makes the mutant enzyme a very sluggish catalyst.

Glu64 is also important for the binding of the anticancer prodrug 5FC. The $K_m$ of the E64A mutant enzyme for 5FC increases more than 200-fold in comparison with that of the wild-type enzyme. Because the rate-limiting step in the activation of 5FC by wild-type yCD is product release, the $K_m$ of the enzymatic reaction is a complex parameter, smaller than the $K_d$ for the binding of 5FC.[13] On the other hand, the rate-limiting step for the activation of 5FC by the E64A mutant enzyme must be the chemical transformation. Consequently, 5FC is in rapid equilibrium with its complex with the E64A mutant enzyme, and thus, the $K_m$ and $K_d$ values should be similar. Therefore, the $K_m$ value of the mutant enzyme is a good measure of the affinity of the mutant enzyme for 5FC and should be compared with the $K_d$ value of the wild-type enzyme for the binding of 5FC, which was determined to be 0.19 mM.[13] The ratio of the mutant enzyme's $K_m$ to the wild-type enzyme's $K_d$ is ∼170, indicating that Glu64 contributes to the binding of 5FC by ∼3 kcal/mol. The biochemical result is consistent with the complex of the enzyme with cytosine[11] built based on the crystal structure of the complex of yCD with the hydrated Py.[5,6] After energy minimization, Glu64 forms a H-bond with the amino group of cytosine. Disruption of the H-bond by mutagenesis is likely to decrease the affinity of the enzyme for the substrate.

yCD belongs to a family of purine/pyrimidine deaminases with an active center featuring a catalytic zinc coordinated with cysteine and histidine residues and a strictly conserved glutamate. Interestingly, yCD is not homologous to eCD, which has a very different size, a different quaternary structure,

and an active center containing a ferrous iron ion coordinated with four histidine residues, an aspartate residue, and a water molecule.[4] Among the family of purine/pyrimidine deaminases, yCD is most similar to *E. coli* cytidine deaminase (CDA), having a catalytic Zn of the same coordination chemistry and a superimposable glutamate.[5,6] However, the functional role of Glu64 of yCD is not the same as that of the corresponding residue Glu104 of *E. coli* CDA, based on our studies on yCD presented here and the published mutagenesis study on *E. coli* CDA.[39] Both glutamate residues are critical for catalyzing their respective reactions. The E104A mutation of *E. coli* CDA decreases the $k_{cat}$ of the enzyme by 8 orders of magnitude.[39] The effect is more dramatic than that of the E64A mutation of yCD, which decreases the $k_{cat}$ of yCD by 5 orders of magnitude and the rate constant for the chemical transformation by 6 orders of magnitude. Similarly, the fluorinated transition-state analogue 5-fluoropyrimidin-2-one riboside is in the hydrated form when bound to the wild-type *E. coli* CDA but is in the unhydrated form when bound to the E104A mutant enzyme,[35] suggesting that Glu104 also plays a critical role in the generation of the reaction intermediate in the deamination reaction catalyzed by *E. coli* CDA.

The roles of the two glutamate residues in substrate binding are different. Glu64 of yCD contributes to the stability of the yCD complex with 5FC by ~3 kcal/mol, as discussed earlier. In contrast, Glu104 of *E. coli* CDA destabilizes the substrate complex of the enzyme *E. coli* CDA.[39] Thus, the $K_m$ of the E104A mutant enzyme decreases by a factor of ~30. Interestingly, the $K_d$ for the binding of the fluorinated transition-state analogue 5-fluoropyrimidin-2-one riboside to the E104A mutant enzyme is even lower than that for its binding to the wild-type enzyme, although the fluorinated transition-state analogue is in the unhydrated form when bound to the mutant enzyme, suggesting that Glu104 of *E. coli* CDA dramatically destabilizes the complex of the unhydrated form of the analogue with the enzyme. It has been proposed that Glu104 of *E. coli* CDA decreases the energy barrier of the deamination reaction not only by stabilizing the transition state but also by destabilizing the enzyme−substrate complex.[35] The destabilization of the enzyme−substrate complex is probably due to the unfavorable interaction between the negatively charged Glu104 and the lone pair of electrons of N3 of cytidine, which becomes a favorable interaction when N3 is protonated during the deamination reaction. *E. coli* CDA can afford this sacrifice of substrate binding energy for the reduction of the energy barrier of the deamination reaction, because the ribose moiety of cytidine contributes to the binding energy for the formation of the enzyme−substrate complex, and consequently, the enzyme is still able to maintain its $K_m$ in the submillimolar range even with the unfavorable interaction between the carboxyl group of Glu104 and N3 of cytidine. On the other hand, without a ribose moiety, cytosine needs a favorable interaction with the carboxyl group of Glu64 of yCD, i.e., a H-bond between the amino group of cytosine and the carboxyl group of Glu64 as described earlier, to keep its $K_m$ in the millimolar range. Without this favorable interaction, the $K_m$ increases by more than 1 order of magnitude as shown by this mutagenesis study, and a CD with a $K_m$ in the tens of millimolar range would not be useful for pyrimidine salvage.

Hydrogen bonds play critical roles in protein structure, stability, and function. The energy of a typical H-bond is in the range of 1−5 kcal/mol,[41] which is particularly suitable for dynamic processes such as molecular recognition and conformational transition. Strong H-bonds, e.g., LBHBs, with energies higher than 10 kcal/mol have also been found in proteins. LBHBs are thought to play an important role in the enormous rate enhancement of enzymatic reactions,[42−44] although this proposition is still under debate.[45] Despite the importance of H-bonds, no single experimental method is sufficient for the characterization of the full range of H-bonds in proteins. X-ray crystallography is most frequently used for the determination of H-bonds, but the resolutions of the diffraction data of protein crystals are usually insufficient for the placement of H atoms. In contrast, only distances between H atoms are measured in NMR structure determination, whereas heteroatoms are defined by standard covalent geometry. However, H-bonds can be detected directly by NMR through *trans*-H-bond scalar couplings for small proteins[46] and *trans*-H-bond deuterium/protium (D/H) isotope effects in favorable situations.[36,37] LBHBs in proteins are characterized generally by a combination of X-ray crystallography and NMR,[38] including the distance between the two heteroatoms determined by X-ray crystallography and several parameters measured by NMR, such as proton chemical shift, proton exchange rate protection factor, D/H fractionation factor, and D [or tritium (T)]/H isotope effects. Unfortunately, most of these parameters are difficult to acquire through direct observation of the bridging proton, in particular for the O···H···O type of H-bonds, because of the exchange broadening of the proton resonance and the poor NMR properties of $^{17}O$, the only NMR active isotope of oxygen. We show that LBHBs can also be identified by a new parameter, the *trans*-H-bond D/H isotope effect (Figure 4). Unlike primary isotope effects,[47,48] secondary isotope effects in proteins can be readily measured by IS-TROSY NMR.[20,21]

In conclusion, the combined experimental and computational studies show that Glu64 plays a critical role in the activation of the anticancer prodrug 5FC. It is important not only for the deamination reaction but also for the binding of the substrate. In the deamination reaction, Glu64 facilitates both the formation of the tetrahedral intermediate and its conversion to the product by shuttling protons. Furthermore, it stabilizes the tetrahedral intermediate and the hydrated form of the inhibitor 5FPy, which mimics the transition state and/or the reaction intermediate. In contrast to Glu104 of *E. coli* CDA, which destabilizes the enzyme−substrate complex, Glu64 of yCD is also important for substrate binding. Its contribution to substrate binding is of great physiological significance. Without Glu64, the $K_m$ of the enzyme would be too high for pyrimidine salvage. The carboxylate of Glu64 forms two strong H-bonds with 5F-DHP in the yCD·5F-DHP complex that mimics the transition state or the tetrahedral intermediate of the activation of the prodrug 5FC, and such H-bonds can be readily detected by IS-TROSY NMR.

## ■ ASSOCIATED CONTENT

### Supporting Information

Downfield region of $^1H$ jump−return spectra of apo wild-type yCD and the complexes of wild-type yCD and the E64A mutant enzyme with the inhibitor 5FPy (Figure S1). This material is available free of charge via the Internet at http://pubs.acs.org.

## AUTHOR INFORMATION


### Corresponding Author

*Phone: (517) 353-5282. Fax: (517) 353-9334. E-mail: yanh@msu.edu.

### Present Addresses

[§]Department of Biochemistry and Molecular Biology, Indiana University School of Medicine, Indianapolis, IN 46202.

[∥]Center for Drug Design, University of Minnesota, 516 Delaware St. SE, Minneapolis, MN 55455.



### Funding

This work was supported in part by National Institutes of Health Grant GM51901, the Grant Agency of the Academy of Sciences of the Czech Republic (Projects IAA400400812 and IAA400400908), and the Grant Agency of the Czech Republic (Project 203/09/1627).


## ACKNOWLEDGMENTS


This study made use of a Varian INOVA 600 NMR spectrometer at Michigan State University funded in part by National Science Foundation Grant BIR9512253.


## ABBREVIATIONS

CD, cytosine deaminase; DHP, 4(*R*)-hydroxy-3,4-dihydro-1*H*-pyrimidin-2-one; eCD, *E. coli* cytosine deaminase; 5F-DHP, 4(*R*)-5-fluorohydroxy-3,4-dihydro-1*H*-pyrimidin-2-one; 5F4SU, 5-fluoro-4-thiouracil; 5FC, 5-fluorocytosine; 5FPy, 5-fluoro-1*H*-pyrimidin-2-one; 5FU, 5-fluorouracil; GDEPT, gene-directed enzyme prodrug therapy; IS-TROSY, isotopomer-selective transverse relaxation-optimized spectroscopy; NMR, nuclear magnetic resonance; ONIOM, our own *N*-layered integrated molecular orbital and molecular mechanics; PAGE, polyacrylamide gel electrophoresis; PCR, polymerase chain reaction; PDB, Protein Data Bank; Py, 1*H*-pyrimidin-2-one; SDS, sodium dodecyl sulfate; TLC, thin-layer chromatography; Tris, 2-amino-2-(hydroxymethyl)-1,3-propanediol; yCD, yeast cytosine deaminase.

## REFERENCES


(1) Aghi, M., Hochberg, F., and Breakefield, X. O. (2000) Prodrug activation enzymes in cancer gene therapy. *J. Gene Med. 2*, 148−164.

(2) Greco, O., and Dachs, G. U. (2001) Gene directed enzyme/prodrug therapy of cancer: Historical appraisal and future prospectives. *J. Cell. Physiol. 187*, 22−36.

(3) Both, G. W. (2009) Recent progress in gene-directed enzyme prodrug therapy: An emerging cancer treatment. *Curr. Opin. Mol. Ther. 11*, 421−432.

(4) Ireton, G. C., McDermott, G., Black, M. E., and Stoddard, B. L. (2002) The structure of *Escherichia coli* cytosine deaminase. *J. Mol. Biol. 315*, 687−697.

(5) Ireton, G. C., Black, M. E., and Stoddard, B. L. (2003) The 1.14 angstrom crystal structure of yeast cytosine deaminase: Evolution of nucleotide salvage enzymes and implications for genetic chemotherapy. *Structure 11*, 961−972.

(6) Ko, T.-P., Lin, J.-J., Hu, C.-Y., Hsu, Y.-H., Wang, A. H.-J., and Liaw, S.-H. (2003) Crystal structure of yeast cytosine deaminase. Insights into enzyme mechanism and evolution. *J. Biol. Chem. 278*, 19111−19117.

(7) Kievit, E., Bershad, E., Ng, E., Sethna, P., Dev, I., Lawrence, T. S., and Rehemtulla, A. (1999) Superiority of yeast over bacterial cytosine deaminase for enzyme/prodrug gene therapy in colon cancer xenografts. *Cancer Res. 59*, 1417−1421.

(8) Kievit, E., Nyati, M. K., Ng, E., Stegman, L. D., Parsels, J., Ross, B. D., Rehemtulla, A., and Lawrence, T. S. (2000) Yeast cytosine deaminase improves radiosensitization and bystander effect by 5-fluorocytosine of human colorectal cancer xenografts. *Cancer Res. 60*, 6649−6655.

(9) Hamstra, D. A., Rice, D. J., Fahmy, S., Ross, B. D., and Rehemtulla, A. (1999) Enzyme/prodrug therapy for head and neck cancer using a catalytically superior cytosine deaminase. *Hum. Gene Ther. 10*, 1993−2003.

(10) Johnson, A. J., Ardiani, A., Sanchez-Bonilla, M., and Black, M. E. (2011) Comparative analysis of enzyme and pathway engineering strategies for 5FC-mediated suicide gene therapy applications. *Cancer Gene Ther. 18*, 533−542.

(11) Sklenak, S., Yao, L. S., Cukier, R. I., and Yan, H. G. (2004) Catalytic mechanism of yeast cytosine deaminase: An ONIOM computational study. *J. Am. Chem. Soc. 126*, 14879−14889.

(12) Yao, L. S., Sklenak, S., Yan, H. G., and Cukier, R. I. (2005) A molecular dynamics exploration of the catalytic mechanism of yeast cytosine deaminase. *J. Phys. Chem. B 109*, 7500−7510.

(13) Yao, L. S., Li, Y., Wu, Y., Liu, A. Z., and Yan, H. G. (2005) Product release is rate-limiting in the activation of the prodrug 5-fluorocytosine by yeast cytosine deaminase. *Biochemistry 44*, 5940−5947.

(14) Yao, L. S., Yan, H. G., and Cukier, R. I. (2006) A combined ONIOM quantum chemical-molecular dynamics study of zinc-uracil bond breaking in yeast cytosine deaminase. *J. Phys. Chem. B 110*, 26320−26326.

(15) Yao, L. S., Yan, H. G., and Cukier, R. I. (2007) A molecular dynamics study of the ligand release path in yeast cytosine deaminase. *Biophys. J. 92*, 2301−2310.

(16) Xu, Q., Guo, H. B., Gorin, A., and Guo, H. (2007) Stabilization of a transition-state analogue at the active site of yeast cytosine deaminase: Importance of proton transfers. *J. Phys. Chem. B 111*, 6501−6506.

(17) Felczak, K., Bretner, M., Kulikowski, T., and Shugar, D. (1993) High-yield regioselective thiation of biologically important pyrimidinones, dihydropyrimidinones and their ribo, 2′-deoxyribo and 2′,3′-dideoxyribo nucleosides. *Nucleosides Nucleotides 12*, 245−261.

(18) Driscoll, J. S., Marquez, V. E., Plowman, J., Liu, P. S., Kelley, J. A., and Barchi, J. J. Jr. (1991) Antitumor properties of 2(1H)-pyrimidinone riboside (zebularine) and its fluorinated analogs. *J. Med. Chem. 34*, 3280−3284.

(19) Cheng, Y. C., and Prussof, W. H. (1973) Relationship between the inhibition constant (ki) and the concentration of inhibitor which causes 50% inhibition (I50) of an enzymatic reaction. *Biochem. Pharmacol. 22*, 3099−3108.

(20) Liu, A. Z., Li, Y., Yao, L. S., and Yan, H. G. (2006) Simultaneous NMR assignment of backbone and side chain amides in large proteins with IS-TROSY. *J. Biomol. NMR 36*, 205−214.

(21) Liu, A. Z., Yao, L. S., Li, Y., and Yan, H. G. (2007) TROSY of side-chain amides in large proteins. *J. Magn. Reson. 186*, 319−326.

(22) Humbel, S., Sieber, S., and Morokuma, K. (1996) The IMOMO method: Integration of different levels of molecular orbital approximations for geometry optimization of large systems: Test for n-butane conformation and $s_n2$ reaction: Rcl+cl. *J. Chem. Phys. 105*, 1959−1967.

(23) Kuno, M., Hannongbua, S., and Morokuma, K. (2003) Theoretical investigation on nevirapine and HIV-1 reverse transcriptase binding site interaction, based on ONIOM method. *Chem. Phys. Lett. 380*, 456−463.

(24) Maseras, F., and Morokuma, K. (1995) IMOMM: A new integrated ab initio plus molecular mechanics geometry optimization scheme of equilibrium structures and transition-states. *J. Comput. Chem. 16*, 1170−1179.

(25) Svensson, M., Humbel, S., Froese, R. D. J., Matsubara, T., Sieber, S., and Morokuma, K. (1996) ONIOM: A multilayered integrated mo+mm method for geometry optimizations and single point energy predictions. A test for Diels-Alder reactions and $Pt(P(t\text{-}Bu)_3)_2 + H_2$ oxidative addition. *J. Phys. Chem. 100*, 19357−19363.

(26) Svensson, M., Humbel, S., and Morokuma, K. (1996) Energetics using the single point IMOMO (integrated molecular orbital plus

molecular orbital) calculations: Choices of computational levels and model system. *J. Chem. Phys. 105*, 3654−3661.
(27) Vreven, T., Mennucci, B., da Silva, C. O., Morokuma, K., and Tomasi, J. (2001) The ONIOM-PCM method: Combining the hybrid molecular orbital method and the polarizable continuum model for solvation. Application to the geometry and properties of a merocyanine in solution. *J. Chem. Phys. 115*, 62−72.
(28) Vreven, T., and Morokuma, K. (2000) On the application of the IMOMO (integrated molecular orbital plus molecular orbital) method. *J. Comput. Chem. 21*, 1419−1432.
(29) Vreven, T., Morokuma, K., Farkas, O., Schlegel, H. B., and Frisch, M. J. (2003) Geometry optimization with QM/MM, ONIOM, and other combined methods. I. Microiterations and constraints. *J. Comput. Chem. 24*, 760−769.
(30) Frisch, M. J., Trucks, G. W., Schlegel, H. B., Scuseria, G. E., Robb, M. A., Cheeseman, J. R., Montgomery, J. A., Jr., Vreven, T., Kudin, K. N., Burant, J. C., Millam, J. M., Iyengar, S. S., Tomasi, J., Barone, V., Mennucci, B., Cossi, M., Scalmani, G., Rega, N., Petersson, G. A., Nakatsuji, H., Hada, M., Ehara, M., Toyota, K., Fukuda, R., Hasegawa, J., Ishida, M., Nakajima, T., Honda, Y., Kitao, O., Nakai, H., Klene, M., Li, X., Knox, J. E., Hratchian, H. P., Cross, J. B., Adamo, C., Jaramillo, J., Gomperts, R., Stratmann, R. E., Yazyev, O., Austin, A. J., Cammi, R., Pomelli, C., Ochterski, J. W., Ayala, P. Y., Morokuma, K., Voth, G. A., Salvador, P., Dannenberg, J. J., Zakrzewski, V. G., Dapprich, S., Daniels, A. D., Strain, M. C., Farkas, O., Malick, D. K., Rabuck, A. D., Raghavachari, K., Foresman, J. B., Ortiz, J. V., Cui, Q., Baboul, A. G., Clifford, S., Cioslowski, J., Stefanov, B. B., Liu, G., Liashenko, A., Piskorz, P., Komaromi, I., Martin, R. L., Fox, D. J., Keith, T., Al-Laham, M. A., Peng, C. Y., Nanayakkara., A., Challacombe, M., Gill, P. M. W., Johnson, B., Chen, W., Wong, M. W., Gonzalez, C., and Pople, J. A. (2003) *Gaussian 03*, revision b.05, Gaussian, Inc., Wallingford, CT.
(31) Becke, A. D. (1993) Density-functional thermochemistry. 3. The role of exact exchange. *J. Chem. Phys. 98*, 5648−5652.
(32) Lee, C. T., Yang, W. T., and Parr, R. G. (1988) Development of the colle-salvetti correlation-energy formula into a functional of the electron-density. *Phys. Rev. B 37*, 785−789.
(33) Stewart, J. J. P. (1989) Optimization of parameters for semiempirical methods. 1. Method. *J. Comput. Chem. 10*, 209−220.
(34) Stewart, J. J. P. (1989) Optimization of parameters for semiempirical methods. 2. Applications. *J. Comput. Chem. 10*, 221−264.
(35) Carlow, D. C., Short, S. A., and Wolfenden, R. (1996) Role of glutamate-104 in generating a transition state analogue inhibitor at the active site of cytidine deaminase. *Biochemistry 35*, 948−954.
(36) Liu, A. Z., Lu, Z. W., Wang, J. F., Yao, L. S., Li, Y., and Yan, H. G. (2008) NMR detection of bifurcated hydrogen bonds in large proteins. *J. Am. Chem. Soc. 130*, 2428−2429.
(37) Liu, A. Z., Wang, J. F., Lu, Z. W., Yao, L. S., Li, Y., and Yan, H. G. (2008) Hydrogen-bond detection, configuration assignment and rotamer correction of side-chain amides in large proteins by NMR spectroscopy through protium/deuterium isotope effects. *ChemBioChem 9*, 2860−2871.
(38) Mildvan, A. S., Harris, T. K., and Abeygunawardana, C. (1999) Nuclear magnetic resonance methods for the detection and study of low-barrier hydrogen bonds on enzymes. *Methods Enzymol. 308*, 219−245.
(39) Carlow, D. C., Smith, A. A., Yang, C. C., Short, S. A., and Wolfenden, R. (1995) Major contribution of a carboxymethyl group to transition-state stabilization by cytidine deaminase: Mutation and rescue. *Biochemistry 34*, 4220−4224.
(40) Yuan, C. H., Tu, S. J., Gelb, M. H., and Tsai, M. D. (2005) Unusual four-bond secondary H/D isotope effect supports a short-strong hydrogen bond between phospholipase A(2) and a transition state analogue inhibitor. *Biochemistry 44*, 4748−4754.
(41) Hibbert, F., and Emsley, J. (1990) Hydrogen bonding and chemical reactivity. *Adv. Phys. Org. Chem. 26*, 255−379.
(42) Cleland, W. W., Frey, P. A., and Gerlt, J. A. (1998) The low barrier hydrogen bond in enzymatic catalysis. *J. Biol. Chem. 273*, 25529−25532.
(43) Cleland, W. W., and Kreevoy, M. M. (1994) Low-barrier hydrogen-bonds and enzymatic catalysis. *Science 264*, 1887−1890.
(44) Frey, P. A. (2001) Strong hydrogen bonding in molecules and enzymatic complexes. *Magn. Reson. Chem. 39*, S190−S198.
(45) Schutz, C. N., and Warshel, A. (2004) The low barrier hydrogen bond (LBHB) proposal revisited: The case of the Asp...His pair in serine proteases. *Proteins 55*, 711−723.
(46) Grzesiek, S., Cordier, F., Jaravine, V., and Barfield, M. (2004) Insights into biomolecular hydrogen bonds from hydrogen bond scalar couplings. *Prog. Nucl. Magn. Reson. Spectrosc. 45*, 275−300.
(47) Cassidy, C. S., Lin, J., and Frey, P. A. (2000) The deuterium isotope effect on the NMR signal of the low-barrier hydrogen bond in a transition-state analog complex of chymotrypsin. *Biochem. Biophys. Res. Commun. 273*, 789−792.
(48) Westler, W. M., Frey, P. A., Lin, J., Wemmer, D. E., Morimoto, H., Williams, P. G., and Markley, J. L. (2002) Evidence for a strong hydrogen bond in the catalytic dyad of transition-state analogue inhibitor complexes of chymotrypsin from proton-triton NMR isotope shifts. *J. Am. Chem. Soc. 124*, 4196−4197.